

Testing Chern-Simons gravity with black holes?

F H Vincent¹

¹ Nicolaus Copernicus Astronomical Center, ul. Bartycka 18, PL-00-716 Warszawa, Poland

E-mail: fvincent@camk.edu.pl

Abstract.

We investigate the possibility to distinguish the small-coupling, slow-rotation black hole solution of Chern-Simons (CS) gravity from the Kerr solution. We develop simulations of electromagnetic observables in the vicinity of CS and Kerr black holes. We show that the typical relative observable difference between CS and Kerr spacetimes is of the order of 0.1% thus beyond reach of current or near-future instruments.

PACS numbers: 04.25.D-, 95.30.Sf

1. Introduction

General relativity (GR) has so far passed all tests with flying colors [1]. However, it remains to be more thoroughly tested in the strong-field regime. Black holes (BH) are a perfect environment for such tests, being the most compact astrophysical objects. In this article, we examine the possibility to distinguish GR from an alternative theory of gravitation that attracted considerable attention recently, Chern-Simons (CS) dynamical gravity [2].

We study here the observable properties of the *slowly rotating* black hole solution derived recently in Refs [3, 4], in the limit of a *small coupling* (see a precise definition below). We restrict ourselves to the *electromagnetic signatures* of both classes of BH, stellar-mass and supermassive ones. In this perspective, we will focus on studying the effect of CS gravity on:

- the Galactic center supermassive BH Sgr A* silhouette,
- the continuous X-ray flux of stellar-mass black holes in X-ray binaries,
- the iron line profile of both classes of BH,
- the quasi-periodic oscillations of both classes of BH.

Our aim is to present a quantitative analysis of the impact of CS gravity on all these observables in order to determine whether current or near-future electromagnetic observations could allow distinguishing between GR and CS gravity.

Few studies have been devoted so far to the electromagnetic signatures of CS gravity. Two recent studies have been dedicated to the difference of flux emitted by a thin

accretion disk surrounding a Kerr or CS black hole [5] and to the impact of CS gravity on the silhouette of a BH [6]. Our aim is to give a broader description of electromagnetic signatures of CS slowly rotating BH and to formulate the results in a format that can be readily compared to real observed data.

Section 2 briefly describes Chern-Simons dynamical gravity. Section 3 presents the slowly rotating CS black-hole solution and geodesic motion in such a spacetime. Section 4 analyzes various electromagnetic signatures of CS slowly rotating BH and section 5 gives conclusions and perspectives.

2. Dynamical Chern-Simons gravity

Dynamical Chern-Simons gravity is described by the action

$$S = S_{\text{EH}} + S_{\text{CS}} + S_{\vartheta} + S_{\text{mat}} \quad (1)$$

where the right-hand terms are defined below. The action

$$S_{\text{EH}} = \kappa \int dx^4 \sqrt{-g} R \quad (2)$$

is the Einstein-Hilbert action, with $\kappa = 1/16\pi$ (here and in the following, we use units in which $c = G = 1$), g being the metric determinant and R the Ricci scalar. The CS correction is described by

$$S_{\text{CS}} = \frac{\alpha}{4} \int dx^4 \sqrt{-g} \vartheta {}^*RR \quad (3)$$

with α being a coupling constant, ϑ the CS coupling scalar field describing deformation from GR (a constant ϑ reduces CS gravity to GR), and ${}^*RR = 1/2 \epsilon^{\alpha\beta\mu\nu} R_{\alpha\beta\gamma\delta} R^{\gamma\delta}{}_{\mu\nu}$ is the Pontryagin density defined by the contraction of the Riemann tensor and its dual, ϵ being the Levi-Civita tensor. The action

$$S_{\vartheta} = -\frac{\beta}{2} \int dx^4 \sqrt{-g} [g^{\mu\nu} \nabla_{\mu} \vartheta \nabla_{\nu} \vartheta + 2V(\vartheta)] \quad (4)$$

is the scalar field action, sum of a kinetic and potential terms, with β being a coupling constant. Finally

$$S_{\text{mat}} = \int dx^4 \sqrt{-g} \mathcal{L}_{\text{mat}} \quad (5)$$

is the matter action.

In the perspective of testing the theory, it is important to constrain the coupling constants. It is useful to introduce two other coupling parameters:

$$\xi \equiv \frac{\alpha^2}{\kappa \beta} \quad (6)$$

has the dimension of L^4 , where L is a unit of length. CS gravity reduces to GR in the limiting case $\xi = 0$. The dimensionless parameter

$$\zeta \equiv \frac{\xi}{M^4}, \quad (7)$$

which scales with the typical mass M of the system, will appear in the expression of the metric for slowly rotating CS black holes. The slowly rotating BH solution found in Refs. [3, 4] is only valid in the limit of small coupling : $\zeta \ll 1$.

To date the best constraint on the coupling constant of the theory is given by [7]

$$\xi^{1/4} \lesssim 10^8 \text{ km.} \quad (8)$$

Note that a much more stringent limit was provided by Ref. [3] but assuming that the exterior metric of a CS neutron star can be described by the slowly rotating BH metric, which is not the case as demonstrated in Ref. [7]. The corresponding dimensionless coupling parameter is restricted to $\zeta \lesssim 10^7$ for a $10^6 M_\odot$ BH, and to $\zeta \lesssim 10^{27}$ for a $10 M_\odot$ BH. The only coupling limit that we will consider in this article is thus the small-coupling condition $\zeta \ll 1$.

3. Geodesic motion around Chern-Simons slowly rotating black holes

3.1. Slowly rotating CS black holes

The metric of a slowly rotating CS black hole is given by [3, 4]

$$\begin{aligned} ds^2 = & - \left(f + \frac{2a^2}{r^3} \cos^2 \theta \right) dt^2 \\ & + \left(\frac{1}{f} - \frac{a^2}{fr^2} \left[\frac{1}{f} - \cos^2 \theta \right] \right) dr^2 \\ & + (r^2 + a^2 \cos^2 \theta) d\theta^2 \\ & + \left(r^2 + a^2 \left[1 + \frac{2}{r} \sin^2 \theta \right] \right) d\varphi^2 \\ & + \left(-\frac{4a}{r} \sin^2 \theta + \frac{5a\zeta}{8r^4} \left[1 + \frac{12}{7r} + \frac{27}{10r^2} \right] \sin^2 \theta \right) dt d\varphi \end{aligned} \quad (9)$$

where $f = 1 - 2/r$, and we have chosen units in which the black hole mass M is unity. Here the metric signature is $(-, +, +, +)$. Note that this metric reduces to the slow-rotation limit of the Kerr metric when $\zeta = 0$, and that the above solution is only correct in the limit $\zeta \ll 1$, $a \ll 1$. Only the $g_{t\varphi}$ term of the metric is modified, and it is very clear that only strong-field phenomena will allow distinguishing this solution from the Kerr solution as the CS correction to $g_{t\varphi}$ is strongly damped by a $1/r^4$ factor.

3.2. Equation of geodesics

Let us consider a particle with mass μ in the spacetime described above. Its specific energy $E = -u_t$ and specific angular momentum $L = u_\varphi$ are conserved in geodesic motion. The geodesic equation reads [8]

$$\begin{aligned}
\Sigma \dot{t} &= \left[-a (aE \sin^2 \theta - L) + (r^2 + a^2) \frac{P}{\Delta} \right] + \Sigma L \delta_{\text{CS}}, \\
\Sigma^2 \dot{r}^2 &= [P^2 - \Delta \{ \mu^2 r^2 + (L - aE)^2 + Q \}] + 2ELf \Sigma^2 \delta_{\text{CS}}, \\
\Sigma^2 \dot{\theta}^2 &= \left[Q - \cos^2 \theta \left\{ a^2 (\mu^2 - E^2) + \frac{L^2}{\sin^2 \theta} \right\} \right], \\
\Sigma \dot{\varphi} &= \left[- \left(aE - \frac{L}{\sin^2 \theta} \right) + \frac{a}{\Delta} P \right] - \Sigma E \delta_{\text{CS}}.
\end{aligned} \tag{10}$$

where $\Sigma = r^2 + a^2 \cos^2 \theta$, $\Delta = r^2 - 2r + a^2$, $P = E(r^2 + a^2) - aL$ and Q is the Carter constant, that is still conserved in CS slowly rotating black hole solution with the same expression as in Kerr. The CS correction term reads [8]

$$\delta_{\text{CS}} = \frac{a\zeta}{112 r^8 f} (70 r^2 + 120 r + 189). \tag{11}$$

The quantities appearing in brackets on the right-hand sides of equation (10) are the standard Kerr geodesic equation. To ease the interpretation of the above equations, these Kerr terms were not approximated by their slow-rotation expression. This approximation was done to obtain the results presented in Section 4.

3.3. Quasi-circular motion

The results presented in Section 4 imply computing some standard quantities of quasi-circular motion in an axially-symmetric stationary spacetime. For completeness the expressions of these quantities are given here. Most of them are taken from Refs. [9, 5].

4-velocity of circular motion The 4-velocity of a massive particle orbiting around a BH in exactly circular motion, is

$$\mathbf{u} = u^t (1, 0, 0, \Omega) \tag{12}$$

where

$$\begin{aligned}
\Omega &= \frac{-g_{t\varphi,r} + \sqrt{(g_{t\varphi,r})^2 - g_{tt,r}g_{\varphi\varphi,r}}}{g_{\varphi\varphi,r}} \\
u^t &= \frac{1}{\sqrt{-g_{tt} - 2g_{t\varphi}\Omega - g_{\varphi\varphi}\Omega^2}}
\end{aligned} \tag{13}$$

Innermost stable circular orbit The radius of the innermost stable circular orbit (ISCO) is found by imposing that the effective potential and its first and second derivatives are zero. The ISCO radius is thus found to be the non-zero real root of the following equation:

$$E^2 g_{\varphi\varphi,rr} + 2ELg_{t\varphi,rr} + L^2 g_{tt,rr} - (g_{t\varphi}^2 - g_{tt}g_{\varphi\varphi})_{,rr} = 0 \tag{14}$$

where the constant of motion can be related to the metric coefficients:

$$\begin{aligned} E &= - \frac{g_{tt} + g_{t\varphi}\Omega}{\sqrt{-g_{tt} - 2g_{t\varphi}\Omega - g_{\varphi\varphi}\Omega^2}}, \\ L &= \frac{g_{t\varphi} + g_{\varphi\varphi}\Omega}{\sqrt{-g_{tt} - 2g_{t\varphi}\Omega - g_{\varphi\varphi}\Omega^2}}. \end{aligned} \quad (15)$$

Photon orbit Not all values of E and L are allowed for a particle moving on a circular orbit around a BH. In order for equations (15) to be valid, the argument of the square root must be positive. The limiting case of zero denominator corresponds to the circular orbit of a particle with infinite specific energy, thus to a photon orbit. It is the innermost limit of all circular orbits of particles. The radius of the photon orbit is thus the real non-zero root of:

$$g_{tt} + 2g_{t\varphi}\Omega + g_{\varphi\varphi}\Omega^2 = 0. \quad (16)$$

Flux of a geometrically thin disk Ref. [10] gives the expression of the flux emitted by a geometrically thin accretion disk in circular rotation:

$$F(r) = \frac{\dot{M}}{4\pi} \frac{1}{\sqrt{g_{rr}(g_{t\varphi}^2 - g_{tt}g_{\varphi\varphi})}} \frac{-\Omega_{,r}}{(E - \Omega L)^2} \int_{r_{\text{ms}}}^r (E - \Omega L) L_{,r} dr \quad (17)$$

where \dot{M} is the averaged accretion rate and r_{ms} is the ISCO radius (assuming the inner edge of the disk is at ISCO).

Epicyclic pulsations Let us now consider a massive particle in quasi-circular motion. It will oscillate with radial and vertical epicyclic frequencies given by (see [11])

$$\begin{aligned} \omega_r^2 &= \frac{(g_{tt} + \Omega g_{t\varphi})^2}{2g_{rr}} \frac{\partial^2 \mathcal{U}}{\partial r^2} \Big|_l \\ \omega_\theta^2 &= \frac{(g_{tt} + \Omega g_{t\varphi})^2}{2g_{\theta\theta}} \frac{\partial^2 \mathcal{U}}{\partial \theta^2} \Big|_l \end{aligned} \quad (18)$$

where the effective potential \mathcal{U} is given by (see e.g. [12])

$$\mathcal{U} = g^{tt} - 2lg^{t\varphi} + l^2 g^{\varphi\varphi} \quad (19)$$

and $l = L/E$.

All the quantities given above can be computed straightforwardly provided the metric is known. In the next section, they will be computed using the metric (9).

4. Strong-field electromagnetic signatures of Chern-Simons gravity

This section is devoted to determine quantitatively the difference between a CS black hole as described by metric (9) and a Kerr BH of identical spin, for various observables.

In order to abide by the two conditions of slow rotation and small coupling, *we fix the spin and dimensionless coupling parameter to $(a, \zeta) = (0.1, 0.1)$* . These two typical values will allow us to derive *characteristic values of the observable difference between CS slow-rotation small-coupling solution and the Kerr metric*.

All the ray-traced simulations presented in this section were computed using the open-source[‡] code **GYOTO** [13].

4.1. Sgr A* silhouette

Here, we compute the silhouette of the Galactic center black hole Sgr A*, assuming it is surrounded by a geometrically thin, optically thick accretion disk extending from the ISCO to $r = 20$. The flux emitted by such a disk is derived from equation (17). We are interested in determining the difference of angular size of the black hole silhouette between Kerr and CS spacetimes. Let us recall that the angular size of the silhouette of a black hole is *only depending on gravitational effects*, not on the astrophysical assumptions we made on the disk structure and emission (including the assumption that the disk terminates at ISCO). Measuring the size of a black hole silhouette is thus a very powerful, astrophysically-unpolluted probe of spacetime.

Photons contributing to the silhouette of the black hole come at closest approach at a coordinate radius equal to the photon orbit radius. For our choice of parameters, the corotating Kerr and CS photon orbits are located at

$$r_{\text{ph,Kerr}} = 2.88219, \quad r_{\text{ph,CS}} = 2.88287, \quad (20)$$

thus differing by 0.02%. It is very clear from this number only that no difference whatsoever will be observable on the black hole image.

Figure 1 shows the superimposed images of CS and Kerr black holes, together with the null geodesic of a photon contributing to the silhouette. The images of the Kerr and CS black holes are undistinguishable by eye at the resolution of the figure (1000×1000 pixels). The difference between the two images is of order of the pixel size, which is approximately $0.01 \mu\text{as}$, thus far below the resolution of any instrument even of the foreseeable future[§]. The right panel shows that the trajectories of photons that come very close to the black hole, when integrated backward in time from the observer to the disk, are clearly different. However their apparent directions on the observer's sky are the same. Only the intensity transported by these photons will differ, but its value depends on astrophysical assumptions and are not as clear a probe as the angular size of the silhouette.

[‡] Freely accessible at gyoto.obspm.fr.

[§] The Event Horizon Telescope [14] will allow imaging the silhouette of Sgr A* with the resolution of $1 \mu\text{as}$.

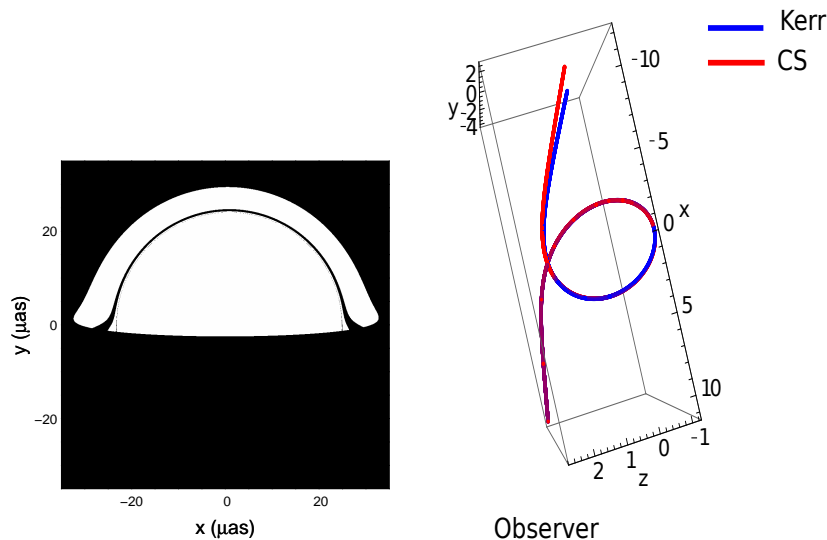


Figure 1. **Left:** superimposition of the images of the innermost part of a geometrically thin optically thick accretion disk around a CS and Kerr black hole at the Galactic center as observed from Earth, with $(a, \zeta) = (0.1, 0.1)$ and an inclination of 85° . The axes are graduated in μas . Illuminated pixels are shown in black whereas non-illuminated pixels are in white color. The silhouette is the thin half-ring of illuminated pixels at the center of the image. The two silhouettes angular sizes are indistinguishable. **Right:** null geodesics of a photon contributing to the silhouette in Kerr (blue) and CS (red) spacetimes. The observer is located downwards. The axes are graduated in natural units ($G = M = c = 1$).

4.2. X-ray flux from stellar-mass black holes

The impact of CS gravity on the X-ray flux emitted by black-hole X-ray binaries is important as these objects are used in order to derive constraints on the Kerr spin parameter through the continuum-fitting technique (for a review, see Ref. [15]), assuming GR is the correct description of gravitation.

Here we consider an optically thick, geometrically thin disk, the inner radius of which coincides with the ISCO, and with outer radius $20 M$. The ISCO radius in the Kerr and CS cases with our choice of parameters is given by

$$r_{\text{ISCO,Kerr}} = 5.6693, \quad r_{\text{ISCO,CS}} = 5.6698, \quad (21)$$

thus differing by 0.01% (with the CS ISCO greater than the Kerr ISCO). The flux emitted by such a disk is given by equation (17). In order to retrieve a result comparable to observed data, this equation must be multiplied by a factor $c^6/G^2 M^2$. Two parameters must then be chosen, the mass M and accretion rate \dot{M} of the source. Moreover, the source distance D will also appear to get observed flux values. We consider here a typical black-hole X-ray binary with $M = 10 M_\odot$, $\dot{M} = 10^{18} \text{ g s}^{-1}$ and $D = 10 \text{ kpc}$.

The emitted flux F_{em} being known at any point of the disk, the corresponding temperature T is simply given by Stefan-Boltzmann law $F_{\text{em}} = \sigma T^4$ where σ is Stefan-Boltzmann constant. Assuming a blackbody radiation, the spectrum emitted by the

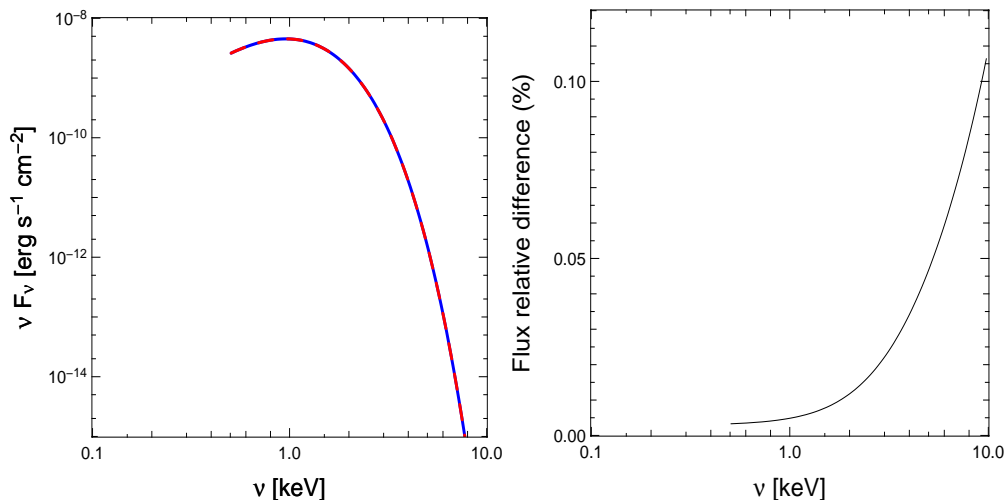


Figure 2. **Left:** X-ray observed spectrum from a Page-Thorne accretion disk surrounding a Kerr (solid blue) or CS (dashed red) black hole with $(a, \zeta) = (0.1, 0.1)$ and an inclination of 45° . **Right:** relative difference between the Kerr and CS fluxes.

disk is then at hand. A practical analytical expression of equation (17) is given in Ref. [10] in the Kerr case, which is thus immediate to compute. In the CS case, we have computed a table of temperature values for a set of radii, and interpolate to get the actual temperature at any point of the disk. Once a map of $B_\nu(T)$ values is computed, where B_ν is the Planck function, the observed flux is computed according to the expression:

$$F_{\nu, \text{obs}} = \sum_{\text{pixels}} B_\nu(T_{\text{pixel}}) \cos\theta \frac{\Delta\Omega}{N_{\text{pixels}}} \quad (22)$$

where the sum is performed over the GYOTO screen containing N_{pixels} pixels, θ is the angle between the normal to the screen and the current pixel direction, and $\Delta\Omega = \pi L^2/D^2$ is the solid angle subtended by the screen which is linked to the field-of-view size L and to the distance of the source D .

Figure 2 shows the spectrum, as observed from Earth, of a typical black-hole X-ray binary in the Kerr and CS cases. The order of magnitude of the flux computed agrees well with real observed data (see e.g. Fig. 6 of Ref. [15]) The right panel shows that the relative difference is of typically 0.05% which makes it impossible to distinguish with current instruments. The increase of the relative difference with frequency is a consequence of the fact that the change of $B_\nu(T)$ with T increases with higher frequencies, for the range of temperatures considered here (i.e. a few 10^6 K). It appears thus that a difference between Kerr and CS thin accretion disks is easier at higher frequency. However, the difference, even at high frequency, stays too low to be observable.

4.3. Iron line profile

Fitting of iron-line profiles is the other commonly used method of fitting spins of black holes (see Ref. [16] for a review). It is thus also important to determine the impact of

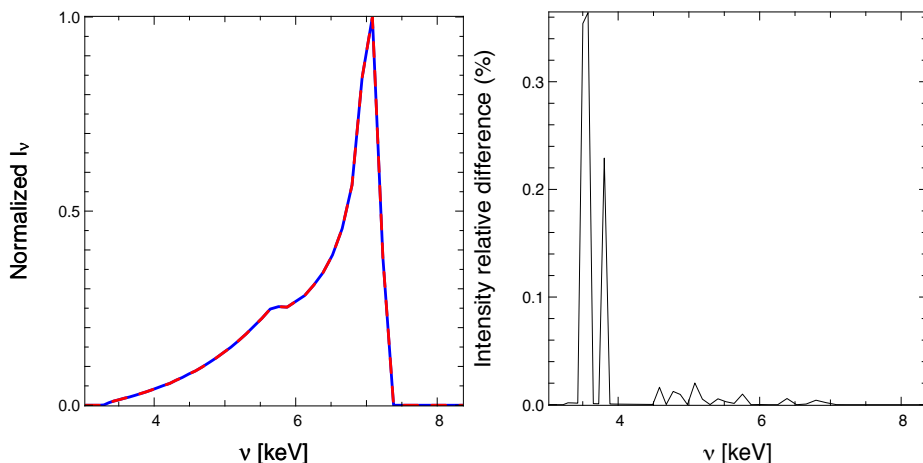


Figure 3. Left: Iron line profile emitted by a geometrically thin disk surrounding a Kerr (solid blue) or CS (dashed red) black hole with $(a, \zeta) = (0.1, 0.1)$ and an inclination of 45° . **Right:** relative difference between the Kerr and CS profiles.

alternative theories of gravitation on this observable.

Following Ref. [16], we model iron lines spectra by considering an optically thick, geometrically thin disk surrounding a black hole extending from the ISCO to an outer radius of $r_{\text{outer}} = 50 M$. The emitted specific intensity is given by

$$I_{\nu, \text{em}} = \delta(\nu - \nu_0) r^{-\beta} \quad (23)$$

where $\beta = 3$, $\nu_0 = 6.4 \text{ keV}$, and δ is the Dirac distribution. For numerical implementation, this distribution is approximated by

$$\delta(\nu - \nu_0) = \begin{cases} 1 & \text{if } |\nu - \nu_0| < 0.01 \nu_0 \\ 0 & \text{else} \end{cases} \quad (24)$$

This choice is linked to the spectral resolution of CHANDRA which is of the order of $E/\Delta E \approx 100$.

Figure 3 shows the corresponding ray-traced iron line profile of the observed specific intensity $I_{\nu, \text{obs}}$, where only the contribution of the primary image was conserved. The overall aspect can be compared to figure 11 of Ref. [16]. The relative difference between the Kerr and CS profiles is of order 0.1%, thus below detection limit. Moreover, the two peaks of relative difference that are the only ones reaching the 0.1% level are due to the limited screen resolution. The height of these peaks is a decreasing function of the number of screen pixels (figure 3 was obtained using 1500×1500 pixels images). This effect is due to the fact that the emitting zone of the disk (i.e. the zone where the emitted frequency is close enough to the line frequency) can be extremely thin projected on the observer's sky for some values of the observed frequency. Then, high resolution is important to resolve these thin areas. Going to even higher resolution would decrease the height of these peaks, but as we are only interested here in determining whether the difference between Kerr and CS gravity is observable, we do not care about the actual height of these peaks.

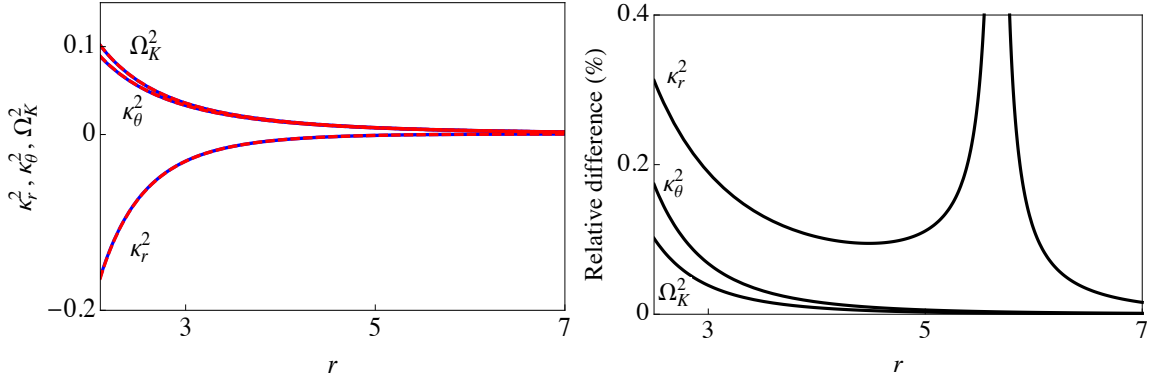


Figure 4. Left: Keplerian (Ω_K) and epicyclic radial (κ_r) and vertical (κ_θ) pulsations profiles for $(a, \zeta) = (0.1, 0.1)$ for Kerr (solid blue) and CS (dashed red) black hole. Natural units $G = M = c = 1$ are used here. **Right:** relative difference between the Kerr and CS profiles. The radial epicyclic pulsation relative difference diverges at ISCO as both Kerr and CS pulsations are zero at this location, and the Kerr and CS ISCO are extremely close.

Let us note finally that given the emitted specific intensity is the same on both cases here, the difference between the two profiles is due to the difference of photon geodesic motion close to the black hole.

4.4. Quasi-periodic oscillations

A few microquasars exhibit high-frequency quasi-periodic oscillations (QPOs) that most probably are linked to strong-field phenomena (for a review, see Refs [17]). The Galactic center flares are also interpreted by some authors as QPOs (see Refs [18, 19] for a review). Many models have been proposed to account for such oscillations, and it is not the aim of this article to review all of them in CS gravity. We will rather restrict ourselves here to two models, namely the epicyclic resonance model [20, 21] and the hot spot model [22].

Epicyclic resonance The epicyclic resonance model suggests that QPOs are due to a resonance between Keplerian and epicyclic frequencies of a particle orbiting in a quasi-circular orbit around a BH. It is thus interesting to determine the relative difference between Kerr and CS epicyclic frequencies: this is shown in figure 4. This figure shows that the relative difference, for the typical spin and coupling parameter chosen in this section, is of order of 0.1% in the very neighborhood of the horizon, decreasing very rapidly when getting further. The difference between epicyclic pulsations is thus below detection level.

Hot spot We have modeled a hot spot orbiting around a black hole following the work presented in Ref. [22]. We consider a timelike geodesic orbiting circularly around a Kerr black hole of spin 0.1 at coordinate radius $r = 7$. The hot spot is defined by a radius

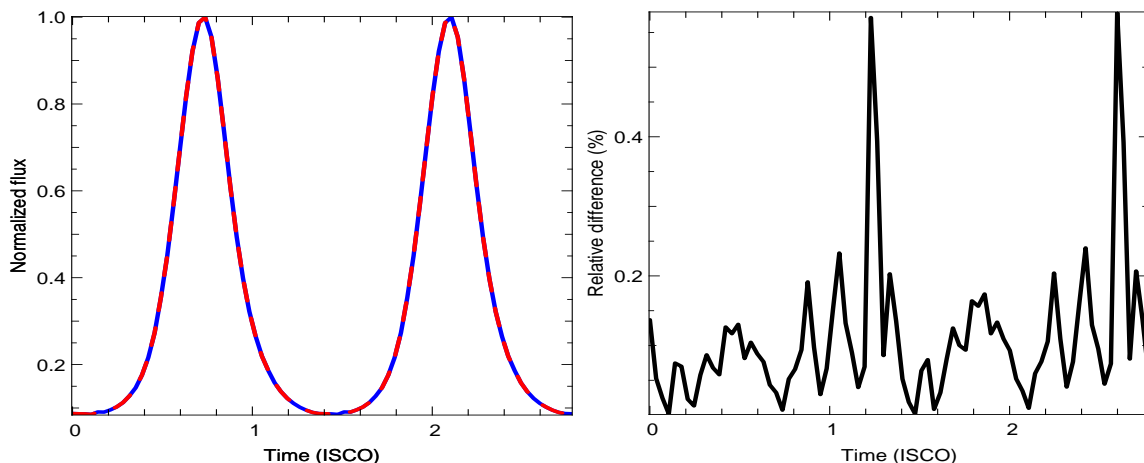


Figure 5. Left: Hot spot light curve for Kerr (solid blue) and CS (dashed red) black hole, for $(a, \zeta) = (0.1, 0.1)$ and an inclination of 45° . **Right:** relative difference between the Kerr and CS light curves. The time unit is the ISCO period for Kerr spacetime with spin 0.1.

$R_{\text{spot}} = 1$. It is assumed to follow the guiding timelike geodesic and to emit radiation isotropically with gaussian modulation of full width at half maximum $\sigma = R_{\text{spot}}/4$. The evolution of such a hot spot is then ray-traced both in Kerr and CS spacetimes, assuming its orbit is inclined at 45° relative to the distant observer. The only difference that affects the simulated light curve is thus the difference of geodesic motion between the two spacetimes. Our interest here is to determine to what level the difference of geodesic motion between Kerr and CS will impact the hot spot observable. Figure 5 shows the hot spot’s light curve for Kerr and CS spacetimes, together with their relative difference. Here as well, the relative difference is of order a few 0.1% which makes it impossible to distinguish with present-day instrumental precision. Moreover, the same remark applies here as for the iron line relative error in figure 3: the two peaks of error that reach the 0.5% level are due to the contribution of the third-order images of the hot spot, which at the resolution used (1000×1000 pixels) are very thin. Thus the height of these peaks depends on resolution, but here again we are only interested in demonstrating that the difference between Kerr and CS spacetimes is beyond instruments’ reach.

5. Conclusion

We have analyzed observables currently proposed as probes of strong-field general relativity in the environment of black holes. Silhouettes, X-ray continuum flux, iron line profile, epicyclic pulsations and hot spot evolution were simulated, both in Kerr and in slow-rotation, small-coupling Chern-Simons gravity. We have determined quantitatively the difference between Kerr and CS predictions, and find that this difference is well below detection limit for all observables, at the maximum level of 0.1%.

Our first conclusion is that slow-rotation, small-coupling CS theory will not be tested by electromagnetic observations in the vicinity of black holes, at least in the

foreseeable future.

Our second conclusion is that in order to determine whether electromagnetic signatures of black holes can help test CS gravity, it is necessary to develop numerical solutions of CS black holes allowing arbitrarily high values of spin. Such solutions would still be at leading order in the coupling constant, as CS gravity is an effective theory (ghosts modes are likely to develop in an exact theory, see the discussion in [23]). It is most probable that higher order perturbative expansion of the solution, as was very recently proposed by Ref. [23], will not change our first conclusion. The metric found by these authors give corrections to the diagonal metric coefficients that can be as high as $1/r$. However, the relative difference $\delta g_{\mu\nu}^{\text{CS},2}/g_{\mu\nu}^{\text{Kerr}}$ of the second-order CS corrections to the Kerr metric coefficients are always of order $1/r^3$ (just as for the ratio $\delta g_{t\varphi}^{\text{CS},1}/g_{t\varphi}^{\text{Kerr}}$ in the first-order solution). Given the extremely small observable differences that we obtained in the first-order expansion, it is unlikely that a second-order treatment would lead to a different conclusion. In order to obtain a more quantitative feeling of the effect of using the second-order CS solution, we computed the relative difference of the radial epicyclic frequency profiles in the Kerr solution and in the second-order CS solution, keeping only the leading-order term in all $g_{\mu\nu}$ coefficients given in Ref. [23]. This relative difference is still of the order of a fraction of a percent, just as in the first-order CS case. Numerical solutions of CS gravity were already derived for slowly rotating black holes, with arbitrary value of the coupling constant [7]. We think that it is in this way that future constraints may be obtained for electromagnetic observables.

Acknowledgments

FHV acknowledges fruitful discussions on CS and other alternative theories of gravitation with W. Kluźniak and M. Abramowicz.

References

- [1] C. M. Will. The Confrontation Between General Relativity and Experiment. *Space Sci. Rev.*, 148:3–13, December 2009.
- [2] S. Alexander and N. Yunes. Chern-Simons modified general relativity. *Phys. Rep.*, 480:1–55, August 2009.
- [3] N. Yunes and F. Pretorius. Dynamical Chern-Simons modified gravity: Spinning black holes in the slow-rotation approximation. *Phys. Rev. D*, 79(8):084043, April 2009.
- [4] K. Konno, T. Matsuyama, and S. Tanda. Rotating Black Hole in Extended Chern-Simons Modified Gravity. *Progress of Theoretical Physics*, 122:561–568, August 2009.
- [5] T. Harko, Z. Kovács, and F. S. N. Lobo. Thin accretion disk signatures in dynamical Chern-Simons-modified gravity. *Classical and Quantum Gravity*, 27(10):105010, May 2010.

- [6] L. Amarilla, E. F. Eiroa, and G. Giribet. Null geodesics and shadow of a rotating black hole in extended Chern-Simons modified gravity. *Phys. Rev. D*, 81(12):124045, June 2010.
- [7] Y. Ali-Haïmoud and Y. Chen. Slowly rotating stars and black holes in dynamical Chern-Simons gravity. *Phys. Rev. D*, 84(12):124033, December 2011.
- [8] C. F. Sopuerta and N. Yunes. Extreme- and intermediate-mass ratio inspirals in dynamical Chern-Simons modified gravity. *Phys. Rev. D*, 80(6):064006, September 2009.
- [9] J. M. Bardeen, W. H. Press, and S. A. Teukolsky. Rotating Black Holes: Locally Nonrotating Frames, Energy Extraction, and Scalar Synchrotron Radiation. *ApJ*, 178:347–370, December 1972.
- [10] D. N. Page and K. S. Thorne. Disk-Accretion onto a Black Hole. Time-Averaged Structure of Accretion Disk. *ApJ*, 191:499–506, July 1974.
- [11] M. A. Abramowicz and W. Kluźniak. Epicyclic Orbital Oscillations in Newton’s and Einstein’s Dynamics. *General Relativity and Gravitation*, 35:69–77, January 2003.
- [12] M. A. Abramowicz. Five Ideas on Black Hole Accretion Disks. In K. Z. Stanek, editor, *The Variable Universe: A Celebration of Bohdan Paczynski*, volume 403 of *Astronomical Society of the Pacific Conference Series*, pages 29–30, March 2009.
- [13] F. H. Vincent, T. Paumard, E. Gourgoulhon, and G. Perrin. GYOTO: a new general relativistic ray-tracing code. *Classical and Quantum Gravity*, 28(22):225011, November 2011.
- [14] S. Doleman et al. Imaging an Event Horizon: submm-VLBI of a Super Massive Black Hole. In *astro2010: The Astronomy and Astrophysics Decadal Survey*, volume 2010 of *Astronomy*, page 68, 2009.
- [15] J. E. McClintock, R. Narayan, S. W. Davis, L. Gou, A. Kulkarni, J. A. Orosz, R. F. Penna, R. A. Remillard, and J. F. Steiner. Measuring the spins of accreting black holes. *Classical and Quantum Gravity*, 28(11):114009, June 2011.
- [16] C. S. Reynolds and M. A. Nowak. Fluorescent iron lines as a probe of astrophysical black hole systems. *Phys. Rep.*, 377:389–466, April 2003.
- [17] R. A. Remillard and J. E. McClintock. X-Ray Properties of Black-Hole Binaries. *ARA&A*, 44:49–92, September 2006.
- [18] R. Genzel, F. Eisenhauer, and S. Gillessen. The Galactic Center massive black hole and nuclear star cluster. *Reviews of Modern Physics*, 82:3121–3195, October 2010.
- [19] M. R. Morris, L. Meyer, and A. M. Ghez. Galactic center research: manifestations of the central black hole. *Research in Astronomy and Astrophysics*, 12:995–1020, August 2012.
- [20] W. Kluzniak and M. A. Abramowicz. Strong-Field Gravity and Orbital Resonance in Black Holes and Neutron Stars — kHz Quasi-Periodic Oscillations (QPO). *Acta Physica Polonica B*, 32:3605, November 2001.

- [21] M. A. Abramowicz and W. Kluźniak. A precise determination of black hole spin in GRO J1655-40. *A&A*, 374:L19–L20, August 2001.
- [22] J. D. Schnittman and E. Bertschinger. The Harmonic Structure of High-Frequency Quasi-periodic Oscillations in Accreting Black Holes. *ApJ*, 606:1098–1111, May 2004.
- [23] K. Yagi, N. Yunes, and T. Tanaka. Slowly rotating black holes in dynamical Chern-Simons gravity: Deformation quadratic in the spin. *Phys. Rev. D*, 86(4):044037, August 2012.